Published in final edited form as:
Neuron. 2011 June 9; 70(5): 908–923. doi:10.1016/j.neuron.2011.05.022.

Experience dictates stem cell fate in the adult hippocampus

Alex Dranovsky[1,6,*], **Alyssa M. Picchini**[1,2,*], **Tiffany Moadel**[1], **Alexander C. Sisti**[1], **Atsushi Yamada**[4,5], **Shioko Kimura**[4], **E. David Leonardo**[1], and **Rene Hen**[1,2,3]

[1] Department of Psychiatry, Columbia University. The New York State Psychiatric Institute, 1051 Riverside Dr., Box 87, New York, NY 10032

[2] Department of Pharmacology, Columbia University. The New York State Psychiatric Institute, 1051 Riverside Dr., Box 87, New York, NY 10032

[3] Department of Neuroscience, Columbia University. The New York State Psychiatric Institute, 1051 Riverside Dr., Box 87, New York, NY 10032

[4] Laboratory of Metabolism, National Cancer Institute, National Institutes of Health, Bethesda, Maryland 20892

Abstract

Adult hippocampal neurogenesis has been implicated in cognitive and emotional processes, and in response to antidepressant treatment. However, little is known about how the adult stem cell lineage contributes to hippocampal structure and function and how this process is modulated by the animal's experience. Here we perform an indelible lineage analysis and report that neural stem cells can produce expanding and persisting populations of not only neurons, but also stem cells in the adult hippocampus. Furthermore, the ratio of stem cells to neurons depends on experiences of the animal or the location of the stem cell. Surprisingly, social isolation facilitated accumulation of stem cells, but not neurons. These results show that neural stem cells accumulate in the adult hippocampus, and that the stem cell-lineage relationship is under control of anatomic and experiential niches. Our findings suggest that, in the hippocampus, fate specification may act as a form of cellular plasticity for adapting to environmental changes.

In the adult hippocampus, the process of neurogenesis (the birth, differentiation, and survival of neurons) is highly susceptible to experimental manipulation of external and internal milieus. Exercise with environmental enrichment (EEE) and antidepressant treatment increase adult hippocampal neurogenesis, while social stress and glucocorticoids decrease it, suggesting that life experiences dictate how adult-born neurons contribute to hippocampal structure and function (Airan et al., 2007; Dranovsky and Hen, 2006; Malberg et al., 2000; Stranahan et al., 2006; van Praag et al., 1999). Adult-born neurons have been causally implicated in specific cognitive and emotional functions (Leuner et al., 2006; Sahay and Hen, 2007; Zhao et al., 2008), and several recent studies have begun to delineate a role for adult hippocampal neurogenesis within normal hippocampal physiology (Clelland et al., 2009; Kitamura et al., 2009; Sahay et al., 2011; Saxe et al., 2006). However, the extent to

[6]Correspondence, requests for materials, and inquiries should be addressed to A.D. (ad722@columbia.edu).
[*]These authors contributed equally to this work.
[5]Present Address: Department of Biochemistry, School of Dentistry, Showa University, 1-5-8 Hatanodai, Shingawa, Tokyo 142-8555, Japan.

which adult-born neurons contribute to normal brain function remains controversial because their contribution to hippocampal structure remains unclear (Breunig et al., 2007).

Adult-born neurons are thought to differentiate from radial astrocyte-like neural stem cells (NSCs) via an intermediate multipotent neuronal progenitor (IP) and become integrated into existing networks (Carlen et al., 2002; Laplagne et al., 2006; Seri et al., 2004; Toni et al., 2008; van Praag et al., 2002). Adult NSCs are currently thought to be a slowly dividing, relatively quiescent reservoir (Encinas et al., 2006), although this notion is beginning to be challenged (Lugert et al., 2010). Mitotic cell label retention studies suggest that some adult-born neurons persist for the life of the animal (Dayer et al., 2003; Doetsch and Hen, 2005). However, mitotic label retention is not informative about populations of cells since a decrease in labeled cells can represent either cell death, or label dilution that accompanies increased division (Breunig et al., 2007). Unlike label retention studies, indelible lineage analysis is a cumulative assessment of cellular populations derived from genetically defined stem cells. Such populations are a summation of the birth and death of all cells within the NSC-derived lineage. Hence, indelible lineage analyses have been successfully used to examine tissue homeostasis (Morrison and Spradling, 2008).

Some indelible lineage studies have been carried out looking at the adult hippocampus (Ahn and Joyner, 2005; Imayoshi et al., 2008; Lagace et al., 2007; Li et al., 2008). However, the results have been widely variable since sensitivity of cellular proliferation to environmental changes renders even subtle experimental differences to manifest in increasingly pronounced changes as the lineage expands over time. Such changes would be especially profound if experimental differences affected the specification of stem cell fate, since directing stem cell fate results in altering the trajectory of the entire derived lineage. Consistent with this notion, indelible lineage analyses from several adult non-neuronal stem cell systems have suggested that changes in the stem cell niche result in modified lineage trajectories and tissue homeostasis (Clayton et al., 2007; Jones et al., 2007; Nakagawa et al., 2007; Ying et al., 2008). Moreover, current lineage-tracing systems have been unsuccessful in restricting genetic recombination to NSCs, targeting both NSCs and rapidly amplifying progenitors and thus limiting the ability to examine how experiences can impact the NSC lineage potential. Given the complexities of indelible lineage studies fundamental questions like, whether adult-born neurons are an accumulating population or if they exist transiently during an immature phase remain unanswered. Therefore, rules governing how changes in the environment result in changes in the cellular composition of the NSC lineage over time are unknown.

Here we report a unique genetic system, which allows indelible lineage analysis from $GFAP^{+}$ radial NSCs, but not from $GFAP^{-}Tbr2^{+}$ neural progenitors. We assessed the contribution of NSCs and their terminal progenies to cellular populations of the hippocampus using an *in vivo* indelible lineage analysis with comprehensive quantification and fate mapping in the adult mouse. Here we report that, in addition to contributing a persistent population of adult-born neurons and undergoing self-renewal, labeled NSCs can accumulate. Remarkably, NSCs in the more active upper blade of the dentate gyrus produced many neurons; consistent with the presence of an intermediate transit amplifying cell (Clayton et al., 2007; Doetsch, 2003; Jones et al., 2007; Nakagawa et al., 2007; Zhao et al., 2008). However, in the less active lower blade a fixed ratio between NSCs and their neuronal progeny made transit amplification less likely. Moreover, manipulating the animal's environment produced fate shifts of the NSC-derived lineage towards a terminal neuronal population in environmentally enriched animals, or an NSC-accumulating population in socially isolated and X-irradiated animals.

We conclude that the lineage relationship between NSCs and their progeny is not fixed, but is dictated by anatomic and experiential niches. Based on our data we propose a model to explain the relationship between NSCs and neurons that may be applicable to understanding tissue homeostasis in other organ systems. We suggest that in the case of adult hippocampal neurogenesis, the NSC-progeny relationship reflects neuronal activity and the animal's experiences, and represents a novel form of neuronal plasticity.

Indelible labeling of adult NSCs

In order to examine how the adult NSC lineage contributes to hippocampal structure we developed a transgenic approach allowing for temporal control of genetic recombination, which is restricted to NSCs (Fig 1). Nestin-CreERT2 mice were generated and bred to an enhanced yellow fluorescent protein (EYFP) reporter line (Srinivas et al., 2001) allowing for indelible lineage tracing analysis in adult mice following administration of tamoxifen (TMX) (Fig 1B, C). We estimated that $EYFP^+$ NSCs were contributing ~50% of total surviving adult-born neurons after lineage equilibrium was achieved (Figure S1F). No EYFP expression was observed 1 or 6 months following vehicle administration (Fig 1D,E). Therefore, the appearance of $EYFP^+$ cells over time was entirely accounted for by the expansion of the $EYFP^+$ lineage after a brief TMX pulse. Moreover, TMX treatment did not result in sustained differences in proliferation (Fig S1E).

Nestin is expressed by both NSCs and intermediate progenitors (Zhao et al., 2008). In order to distinguish which of the two cell types incurred cre-mediated recombination in our system, we used the astrocyte marker GFAP and the intermediate progenitor marker Tbr2. Glial fibrillary acidic protein (GFAP) is expressed by both stem and non-stem astrocytes, which can be distinguished respectively by their radial and stellate morphologies (Seri et al., 2004). Tbr2 was recently established to be predominantly expressed in adult hippocampal IPs, but not NSCs (Hodge et al., 2008). BrdU was administered to the animals to establish which cells were undergoing division around the time recombination took place. 48 hours after TMX and BrdU administration we observed EYFP cytoplasmic staining in the SGZ cell bodies (Fig 1F–J). Quadruple labeling for EYFP, GFAP, Tbr2 and BrdU revealed that most cells undergoing recombination were $GFAP^+$ (Fig 1G,K). In addition to $EYFP^+GFAP^+$ cells in the SGZ, the presence of $EYFP^+GFAP^+$ stellate cells in the molecular layer of in the dentate revealed that recombination was taking place in at least some non-stem astrocytes (Fig 1G). Closer analysis revealed that the majority of cells undergoing recombination were $GFAP^+Tbr2^-BrdU^-$ (Fig 1K) suggesting that recombination did not occur in IPs but was predominant to GFAP-expressing astrocytes that were not undergoing division. While we identified a small number of Tbr2-expressing $EYFP^+$ cells 48 hours after recombination, all $EYFP^+Tbr2^+$ cells were also $GFAP^+$ and $BrdU^+$ (Fig 1G–J). Similarly, all $EYFP^+BrdU^+$ cells were $GFAP^+$ and $Tbr2^+$ (Fig 1G–K). Taken together the results suggest that recombination occurs predominantly in radial astrocytes and that Tbr2 is expressed by dividing radial astrocytes in addition to proliferating IPs.

Given that we observed recombination in stem and non-stem cells, it became critical to establish the identity of the predominant cell type labeled by our system. We first examined if $EYFP^+$ cells in the SGZ also expressed Nestin and GFAP (Fig 2A–D). As expected, 6 days after TMX (when we were first able to detect EYFP in the cellular processes), almost all $EYFP^+$ cells are also $Nestin^+$ (data not shown). Remarkably, almost all $EYFP^+Nestin^+$ cells were also expressing GFAP (Fig 2S), further indicating that recombination was taking place in nestin-expressing NSCs, but not nestin-expressing IPs.

Two developmental lineage studies identified glial fibrillary acidic protein (GFAP) and brain lipid-binding protein (BLBP) as functional stem cell markers during embryonic brain

development (Anthony et al., 2004; Malatesta et al., 2003). We therefore used BLBP along with GFAP and radial morphology to identify EYFP$^+$ NSCs (Figs 2E–H). GFAP and BLBP are also expressed by terminally differentiated stellate astrocytes, which can be readily distinguished from NSCs by expression of non-stem astrocyte marker-S100β (Fig 2I–L). Quantitative analysis revealed that while virtually all EYFP$^+$GFAP$^+$ radial cells also expressed BLBP, none of them expressed S100β (Fig 2Q,R). We could also readily identify stellate EYFP$^+$GFAP$^+$ cells, which were S100β$^+$ (data not shown) and were thus determined to be terminally differentiated astrocytes. Finally, we identified numerous actively dividing EYFP$^+$GFAP$^+$ radial cells using the S-phase marker MCM2 (Fig 2M–P) providing further evidence that EYFP$^+$ NSCs can divide.

Taken together these results established that EYFP$^+$GFAP$^+$ cells with radial morphology could be regarded as NSCs and these criteria were used to identify NSCs in subsequent experiments.

In order to identify cellular populations within the NSC lineage, we performed fate-mapping studies with validated cellular markers and established morphology. Our preliminary analysis revealed that 1 month after recombination, EYFP could be detected in radial (Fig 3A,B) and stellate (Fig 3C) GFAP$^+$ astrocytes, immature doublecortin-expressing neurons (Fig 3D) and mature neurons (Fig 3E). EYFP$^+$ neurons were identified by co-expression of NeuN (Fig 3E), while doublecortin (DCX) was used to identify neuroblasts and immature neurons (Fig 3D) (Ming and Song, 2005). Fate mapping analysis of the EYFP$^+$ cells as they emerged after TMX treatment revealed that initially radial NSCs constituted 75% of EYFP$^+$ cells (Fig 3F). EYFP$^+$GFAP$^-$DCX$^-$ round cells constituted the 2nd largest population. Immature neurons (EYFP$^+$DCX$^+$) began to accumulate after 2 weeks (Fig 3F) with EYFP$^+$DCX$^+$NeuN$^-$ neuroblasts preceeding EYFP$^+$DCX$^+$NeuN$^+$ maturing neurons (Fig S2A). Moreover, EYFP$^+$ axons were detected within 2 weeks in the major dentate gyrus output tracts (mossy fibers) and increasingly represented over the course of a month following TMX (Fig S2B–H). Taken together, our studies indicated that TMX induces EYFP expression in mostly NSCs, which have a lineal relationship with the major cell types previously reported to comprise the adult hippocampal NSC lineage: intermediate progenitors, immature neurons, mature neurons, and non-stem astrocytes.

We next performed a quantitative evaluation of the NSC lineage over the course of the animals' adult life. Prior studies have reported that many of the adult-born neurons do not survive to maturity, but cells that survive for four weeks are likely to be present one year later (Kempermann et al., 2003). Adult animals were administered TMX and sacrificed after 1, 3, 6, or 12 months of standard laboratory housing. We noted an accumulation of the EYFP$^+$ cells as the animals aged (Fig 4A–D). We also observed a previously reported decrease in DCX$^+$ cells between the 3 and 6-month-old animals (1 and 3 months groups, Fig 4E,F) and between the 9 and 15-month-old animals (6 and 12 months groups, Fig 4G,H). Interestingly, in 15-month-old animals (12 months group) the NSC-derived lineage persisted despite sparse neurogenesis as indicated by few DCX$^+$ immature neurons (Fig 4H).

Currently, the majority of adult-born hippocampal cells are thought to become neurons derived from relatively quiescent NSCs via transit amplifying IPs (Doetsch and Hen, 2005; Kempermann et al., 2006; Kempermann et al., 1997; Ming and Song, 2005). We thus expected to see an increase in the proportion of neurons with a corresponding decline in the proportion of NSCs within the EYFP$^+$ lineage over time. Neurons did constitute the largest proportion of the EYFP$^+$ lineage, with GFAP$^+$ NSCs, GFAP$^+$ stellate astrocytes, and GFAP$^-$DCX$^-$NeuN$^-$ cells constituting the other cell types (Fig 4I). Very few DCX$^+$ cells were NeuN$^-$ (data not shown). This group was therefore not included as a separate population in the analyses. Surprisingly, we detected no difference in the relative

representation of each cellular population within the lineage over time until the last time point measured, where the neuronal contribution increased [$t(8)=-2.34$, $p=.047$] (Fig 4J). Since the NSC-derived lineage appeared to be accumulating over the time course (Fig 4A–D) during which the proportion of NSCs remained the same (Fig 4J), the intriguing possibility that the number of NSCs within the lineage was increasing emerged.

In order to assess the lineage potential of $EYFP^+$ NSCs, we performed unbiased stereological analysis. We noted an accumulation of the total number of $EYFP^+$ cells (Fig S3A) and the populations represented within it (Fig 4I). Approximately 15,000 neurons were added to the dentate gyrus between 3 and 9 months of age based on our estimate that $EYFP^+$ neurons constituted ~50% of neurons born after TMX (Fig S1F). The effect of time for our 4 groups was significant for NSCs: $F(3,12)=6.67$, $p=0.007$, and for neurons after excluding the 12-month group $F(2,9)=17.15$, $p=0.002$. The 12-months neuron group was excluded from the analysis due the large variance in neurons, but not other lineage populations in this group (Fig. 4I). Different variances in NSC and neuronal $EYFP^+$ populations within one group indicated that the relationship between NSCs and their terminal progenies is not fixed in older animals. In summary, restricting genetic labeling to NSCs revealed that these cells proliferate, survive and can have highly variable relationships to their neuronal progeny.

NSC location determines its lineage relationship

We next tested the possibility that niche factors can direct the relationship between NSCs and their neuronal progeny. Differences between the upper and lower blades of the dentate gyrus were previously described (Ramirez-Amaya et al., 2006). We observed that $EYFP^+$ NSCs appeared to constitute a greater proportion of $EYFP^+$ cells in the lower than the upper blade (Fig 5A–C). Therefore, we compared stereological analyses between blades (Fig 5D,E). The analysis revealed differences in the number of $EYFP^+$ NSCs, but not neurons or other populations between the upper and lower blades of the dentate 6 months after TMX administration [$t(2)=-5.554$, $p=0.03$]. These results suggested that the lineage relationship between NSCs and their terminal progeny differed between blades of the dentate gyrus. We therefore examined the relationship between NSCs and neurons in each blade of the dentate gyrus (Fig 5F,G). We were surprised to find that the lower blade of the hippocampus had a linear relationship between NSCs and neurons ($p<0.0001$, $R^2=0.80$). No such relationship was observed between NSCs and neurons in the upper blade or the total dentate, suggesting a variable number of symmetric divisions by intermediate cells in the upper blade. These findings suggest that the NSC-progeny relationship can vary greatly and is under regional control.

NSC & neuronal expansion is dissociable

Given that the NSC population was not as quiescent as previously thought, but accumulated over time, we asked if environmental interventions known to affect neurogenesis do so by altering NSC fate. Exposure to X-irradiation blocks neurogenesis and disrupts the neurogenic niche (Monje et al., 2002; Santarelli et al., 2003), while exercise with environmental enrichment (EEE) potently stimulates neurogenesis (Doetsch and Hen, 2005; Dranovsky and Hen, 2006; Ming and Song, 2005; van Praag et al., 1999; Zhao et al., 2008). We reasoned that a single exposure to irradiation, while killing all cells in S-phase, is unlikely to result in the death of slowly dividing cells and could be used to separate the anti-mitotic from the anti-neurogenic effects of X-rays. Mice were subjected to whole brain X-irradiation, followed by treatment with TMX and then either sacrificed or exposed to standard or EEE housing conditions for 1 month (Fig 6A). Exposure to irradiation completely blocked neurogenesis and depleted DCX expression within 2.5 weeks (Fig 6G–I). We observed Cre-mediated recombination in NSCs after irradiation (Fig 6C,K,O)

suggesting that not all cells within the lineage were susceptible to X-ray-induced death and confirming our prior observation that recombination takes place in non-mitotic cells. Moreover, irradiated animals that were allowed to survive 1 month after TMX had more $EYFP^+$ cells than those sacrificed immediately after TMX, demonstrating that the NSC lineage was accumulating over time following X-ray exposure (Fig 6C,D,K,L,O,P). Fate mapping in irradiated animals revealed that almost all $EYFP^+$ cells were $GFAP^+$, and most exhibited radial astrocyte morphology indicating that mostly proliferating NSCs and few astrocytes were being produced by NSCs (Fig 6O,P). These results demonstrate that our X-irradiation protocol completely obliterates the emergence of neurons from NSCs without profoundly altering the ability of NSCs to survive, self-renew, and accumulate. Rather, the effects of X-irradiation are predominantly on neurogenesis.

Sham irradiated animals exposed to EEE had an abundance of DCX^+ and $EYFP^+$ cells (Fig 6F,J). Most of the $EYFP^+$ cells expressed both DCX and NeuN (Fig 6N,R) indicating that mostly neurons are produced in the NSC-derived lineage under EEE conditions. However, the irradiated animals exposed to EEE did not exhibit marked differences in the number of $EYFP^+$ cells from the irradiated cohort exposed to standard housing (Fig 6D,E). Fate mapping revealed that the $EYFP^+$ lineage in irradiated animals exposed to EEE, or to standard housing, consisted primarily of NSCs, with some astrocytes and $EYFP^+GFAP^-DCX^-NeuN^-$ round cells also present (Fig 6L,M,P,Q). Comparison of X- to sham-irradiated animals exposed to EEE revealed a fate shift from a mostly neuronal to a predominantly NSC fate of the lineage (Fig 6B). These results demonstrate that X-irradiation blocks accumulation of neurons, but not NSCs. Since EEE did not profoundly affect expansion of the NSC population, we concluded that NSC and neuronal fate specification is dissociable.

Experiences guide NSC fate & lineage homeostasis

The results above demonstrated that both NSCs and neurons were increasingly represented within the NSC lineage, and that fate specification was dissociable. Moreover, the data suggest that fate specification within the adult-born hippocampal NSC lineage is governed by regional differences. We hypothesized that the NSC lineage potential, NSC-neuron relationship, and ultimately NSC number may be subject to regulation by more naturally occurring experiences. Social isolation was previously demonstrated to decrease cellular proliferation and neurogenesis in the hippocampus (Ibi et al., 2008; Lu et al., 2003) and alter the effects of neurogenesis-promoting experiences (Stranahan et al., 2006). Moreover, increased numbers of $GFAP^+$ cells were reported following adrenalectomy (Gould et al., 1992). We asked if social isolation and EEE induce changes in adult hippocampal neurogenesis by instructing a fate shift within the lineage towards NSC accumulation or neurogenesis. Animals were exposed to either social isolation or EEE, followed by stereology and fate mapping analysis 1 and 3 months after TMX. After 1 month, $EYFP^+$ cells appeared to accumulate in both socially isolated and EEE-exposed animals compared to animals housed under standard laboratory conditions (Fig 7D–F). We noted that while there were fewer DCX^+ cells in socially isolated (Fig 7A) compared to standard housed (Fig 7B) animals, more $EYFP^+$ cells exhibited NSC morphology in the isolated group (Fig 7D). EEE profoundly increased neurogenesis and expanded the $EYFP^+$ lineage (Fig 7C,F). Socially isolated animals had a significant increase in the proportion of $EYFP^+$ NSCs [$t(6)=-3.181$, $p=0.0095$]; while the proportion of $EYFP^+$ neurons was greater in animals exposed to EEE [$t(5)=-3.244$, $p=0.012$] compared to standard-housed animals (Fig 7G). Animals exposed to 1 month EEE also had proportionally fewer $EYFP^+$ NSCs than their standard-housed controls [$t(5)=4.351$, $p=0.004$]. Interestingly, after 3 months of environmental manipulations, there was no significant effect of social isolation on the proportion of $EYFP^+$ NSCs [$t(6)=1.705$ $p=.07$], while effect of EEE on the proportion of $EYFP^+$ neurons was

augmented [$t(4)=-2.820$, $p=0.03$] compared to the 1 month time point (Fig 7H). Following 3 months of EEE, neurons constituted over 80% of the lineage and less than 10% were NSCs.

Unbiased stereological analysis revealed a greater than two-fold increase in the absolute number of $EYFP^+$ NSCs in socially isolated animals compared with standard-housed animals (Fig 7I). This effect was unchanged 3 months later. Following 1 month of EEE, animals exhibited accumulation of $EYFP^+$ neurons [$t(5)=-2.005$, $p=0.05$] compared to standard-housed animals (Fig 7J) surpassing the 6-month peak under standard laboratory housing (Fig 4I). This effect was further amplified following 3 months of EEE with over 70,000 $EYFP^+$ neurons surviving within the lineage. This finding corresponded to a decrease in DCX^+ cells in the 3 months EEE (Fig S7C) compared to the 1 month EEE groups (Fig 7C) suggesting that while the neurogenic effect of EEE reached a plateau by this time, newly generated neurons continued to survive and populate the dentate gyrus. There was no increase in $EYFP^+$ NSCs after 1 month [$t(5)=-1.054$, $p=0.17$] or 3 months [$t(4)=-1.181$, $p=0.15$] of EEE. These results indicate that social isolation and EEE have opposite effects on the fate of the NSC lineage, and that NSC and neuronal accumulation can be dramatically affected by the animal's experience.

Having established regional differences in the potential of NSCs for neurogenesis between the upper and lower blades of standard-housed animals (Fig 5), we next asked if the effects of social isolation and EEE could also direct the fate of the lineage by changing the NSC-neuron relationship. The proclivity of NSCs to produce neurons was compared between socially isolated, standard-housed, and EEE animals by looking at the relationship of NSCs and neurons within the $EYFP^+$ lineage (Fig 7K). The results indicate that EEE exposure promotes a variable relationship between NSCs and their neuronal progeny [$p=0.297$, $R^2=0.264$], dramatically increasing the number neurons that are produced by relatively few NSCs and providing strong support for neurogenesis through a transit amplifying intermediate progenitor. Conversely, in animals exposed to social isolation, NSCs and neurons exhibited a linear relationship [$p=0.056$, $R^2=0.484$] with a slope similar to that found in the lower blade of standard-housed mice. Both EEE and socially isolated animals lost the disparity in the NSC-neuronal homeostasis between upper and lower blades (Fig S6) that was seen in controls (Fig 5F,G). In socially isolated animals 1–2 neurons were produced for every NSC in the total dentate exhibiting a linear stoichiometry unlikely to be associated with a transit-amplifying cell.

Given that many adult-born neurons undergo apoptosis, but there is no direct way to assess cell death over time, we examined if our behavioral interventions could affect cellular survival to account for differences in lineage trajectories (Fig S4A). We found that social isolation did not decrease cellular survival and that enrichment increased survival (Fig S4B) by a magnitude that could not account for the observed lineage gains (Fig 7J,K). We also assessed the numbers of cells undergoing apoptosis at time of sacrifice in each group in this study (Fig S4C–F). We did not detect differences in the number of apoptotic cells between our behavioral interventions (Fig S4C). Moreover, the number of cells undergoing apoptosis did not correlate with accumulation of $EYFP^+$ cells across the groups (Fig S4D). We also did not detect differences in the number of cells undergoing apoptosis between the different age groups used in this study (at different time points) (Fig S4E,F). Thus, social isolation promoted accumulation of $EYFP^+$ NSCs and instructed NSCs towards a linear relationship with their terminal neuronal progeny. EEE promoted accumulation of $EYFP^+$ neurons and instructed NSCs towards a variable relationship with their terminal neuronal progeny.

Discussion

NSCs accumulate in the adult dentate gyrus

Here we report the first system that allows for inducible cre-mediated recombination in adult hippocampal radial GFAP-expressing NSCs, but not GFAP^{-}Tbr2-expressing neural progenitors. Surprisingly, we observed an increase in the absolute number of EYFP^{+} NSCs over time. In the adult brain, radial astrocyte-like stem cells are currently considered to be "quiescent", self-renewing, and are not thought to accumulate (Encinas et al., 2006). One recent lineage study suggested that NSCs undergo a limited and constant number of asymmetric divisions resulting in self-renewal only, followed by differentiation into terminal astrocytes suggesting that NSCs are depleted with age (Encinas et al., 2011). However, an inherent limitation of genetically defined lineage studies is the potential for functional heterogeneity within the genetically defined stem cell. NSC heterogeneity was recently proposed in a report describing a non-radial multipotent cell with astrocyte-like properties (Lugert et al, 2010). While the lineal relationship of these horizontal cells to radial NSCs remains to be established, more horizontal cells were present in animals subjected to experimental seizure protocols. The latter finding suggests a stem cell dormancy hypothesis that is further supported by historical observations that even in aged animals, when baseline proliferation is minimal, EEE induces a robust increase in neurogenesis (Kempermann et al., 1998). The increase in EYFP^{+} NSCs over time reported in this study demonstrates that radial NSCs are not simply self-renewing, but can undergo population expansion, and perhaps, turnover. Whether these proliferating NSCs represent a distinct sub-population of cells, or if the stem cell niche can instruct all NSCs to proliferate remains to be determined.

Lifetime contribution of the NSC lineage

Our comprehensive *in vivo* analysis of the adult-born hippocampal NSC lineage reveals that multiple cellular populations survive for extended periods of time and have the capability to accumulate. Along with the potential to divide, diversity of stem cell progeny can also be instructed by the niche or reflect stem cell heterogeneity. Our results form the basis for an important question: whether the same or different NSCs or IPs produce NSCs, astrocytes, or neurons (Fig 8). Further characterization of the NestinCreERT2 and other genetically defined NSC pools should reveal whether lineage diversity currently ascribed to adult NSCs reflects truly multipotent cells or a heterogeneous pool of committed progenitors and whether all or only some NSCs can proliferate.

We report that modest neurogenesis under standard laboratory housing can dramatically increase to produce over 70,000 neurons within three months under more naturalistic conditions of EEE. Hence, persistent adult-born neurongenesis can make a substantial contribution to the 500,000-neuron dentate gyrus (Abusaad et al., 1999; Kempermann et al., 1998)

Accumulation of EYFP^{+} cells under standard laboratory housing varied greatly with the age of the animals. Age-related decline in adult hippocampal neurogenesis has been well established (Drapeau and Abrous, 2008). Specifically, neurogenesis decreases much more rapidly between the 1 and 3-month groups (3–4 and 5–6 month-old animals) than between the 3 and 6-month groups (5–6 and 8–9 month-old animals) as demonstrated by several groups using different markers (Seki and Arai, 1995; Wu et al., 2008). Thus, any gains in EYFP^{+} cells between 1 and 3 months after TMX are obscured by a logarithmic age-related decline in baseline neurogenesis during this time period. However, gains between 3 and 6 months are readily apparent since neurogenesis becomes more constant in this time period. It is also noteworthy that our study design does not distinguish if one of the genders accounts for the observed differences.

Increased variance in the number of $EYFP^+$ neurons in the 12 months group (Fig 4I) with low variance in the number of $EYFP^+$ NSCs in the same animals revealed that the capacity of NSCs for generation of neurons and/or the viability of adult-born neurons varies greatly in older animals. Similarly, the NSC-neuronal relationship differed between the upper and lower blades of the dentate gyrus and between EEE and socially isolated mice. Remarkably, the NSC-neuronal relationship was linear in the lower blade of the DG, suggesting that in some instances the presence of a dedicated transit amplifying cell is not required to explain the NSC-neuronal relationship as explained below.

Evidence for a more versatile intermediate progenitor

An NSC-progeny relationship that shifts between linear and variable is inconsistent with the current model of adult hippocampal neurogenesis. Similar to the biology of resident stem cells in other organs, NSC division is currently thought to result in a transit amplifying IP cell and another NSC. The IP is then thought to divide symmetrically multiple times before differentiating into its terminal fates and has been termed a “transit-amplifying cell” (Fuchs, 2009; Jones et al., 2007; Zhao et al., 2008). Unlike other stem cells, resident stem cells in the epidermis were recently shown to follow lineage expansion with a linear stoichiometry by which each intermediate progenitor cell divides to produce one intermediate progenitor and one terminally differentiated cell (Clayton et al., 2007). Mathematical modeling suggests that expansion with linear stoichiometry is inconsistent with transit amplification (Clayton et al., 2007; Jones et al., 2007). While linear expansion was reported for epidermal differentiation, expansion through a transit amplifier is observed in models of epidermal injury (Ghazizadeh and Taichman, 2001). These seemingly paradoxical findings have generated a controversy about the homeostasis underlying stem cell differentiation (Jones et al., 2007).

Our results indicate that exposure to different environments can influence the proclivity of NSCs for proliferation versus neurogenesis. This interpretation is most dramatically supported by the results of the X-irradiation experiment where disruption of the NSC niche prevented neurogenesis, but permitted NSC proliferation. Furthermore, we observed a homeostatic shift from linear to a variable NSC-neuronal relationship following more naturalistic environmental manipulations or with a more restricted anatomic analysis of animals exposed to standard laboratory housing. In order to place our findings into the context of reports describing tissue homeostasis in other organs, we propose a new model for adult hippocampal neurogenesis (Fig 8). Our results are most consistent with an intermediate progenitor that can divide to produce neurons or NSCs, or undergo multiple symmetric divisions acting as a transit-amplifying cell. The mode of lineage expansion is dictated by the structural (anatomic) niche and functional changes in the niche resulting from the animals’ experiences. More neurogenesis would be expected under conditions in which symmetric amplification of an IP and terminal differentiation were favored, while less neurogenesis would be associated with accumulation of NSCs. Interestingly, one recent report found that intermediate progenitors can function as transit amplifying cells during spermatogenesis, but produce germ stem cells following stem cell depletion (Nakagawa et al., 2007). It is enticing to speculate that the ability of intermediate progenitors for transit amplification upon demand is a general property of many stem cell systems. Transit amplification was demonstrated in the developing brain by direct visualization of intermediate progenitors undergoing division over time (Noctor et al., 2004). A similar experiment would test our model in the adult hippocampus.

Cell death and cellular turnover within the NSC lineage

Cell survival impacts any lineage as it accumulates, but unfortunately the number of cells undergoing apoptosis over time is difficult to quantify due to transient expression of

apoptotic markers and rapid clearance of dead cells. While some indirect information about cumulative cell death can be achieved through BrdU survival studies, the technique provides limited information about total populations of cells (Taupin, 2007). BrdU survival experiments are least informative about slowly dividing NSC and rapidly dividing IP populations since the former are poorly labeled by BrdU, while decreased label retention in the latter can reflect either cell death or multiple divisions (Dayer et al., 2003; Encinas et al., 2011; Mandyam et al., 2007; Taupin, 2007). Hence, the contributions of NSC and IP cell death during lineage accumulation and in response to environmental manipulations remain to be determined.

Our own cell survival studies of neurons, which are post-mitotic and thus lend themselves to BrdU survival studies did not detect an effect of social isolation on survival (Fig S4A,B). In EEE-treated mice, in addition to observing a well-established and robust increase of proliferation (data not shown), we also detected increased neuronal survival suggesting that decreased neuronal death contributes to the lineage gains described in this study. Our inability to detect any relationship between apoptosis and lineage expansion, within or between any of our groups suggests that apoptosis (Fig S4D,F), while impacting accumulation of the lineage, is unlikely to account for the differences that we observe.

Modification of the NSC lineage as a form of cellular plasticity in the adult brain

An expanding stem cell compartment could allow the brain to grow a NSC reservoir during deprived conditions such as isolation stress. This brain adaptation would then allow an augmented neurogenic response through experience-directed fate specification when the environment became richer. An analogous type of proliferative control was recently recapitulated in a more artificial, embryonic stem cell system where extrinsic stimulation and activation of signaling pathways favored differentiation, while depleting these signals favored self-renewal (Ying et al., 2008). The signals dictating changes in the fate of the NSC lineage remain to be determined. Of particular interest are the multiple observations that neural activity is positively linked to cell division in the adult dentate gyrus (Deisseroth et al., 2004; Tozuka et al., 2005). Environmental enrichment was previously demonstrated to increase neuronal activity in the dentate gyrus (Tashiro et al., 2007) while social isolation was recently demonstrated to decrease it (Ibi et al., 2008). Moreover, baseline differences in neuronal activity were described between the upper (more active) and lower (less active) blades of the dentate gyrus (Ramirez-Amaya et al., 2006). Our observations of a linear relationship between neurons and NSCs in the lower blade and following social isolation in contrast with transit amplifying dynamics in the upper blade and following EEE are consistent with activity differences under these conditions. We suggest that regional differences in baseline neuronal activity and activity changes in response to a changing environment underlie regulation of the NSC lineage. We therefore propose a novel form of cellular plasticity where the brain responds to changes in the environment by shifting the dynamics of both stem cell differentiation and survival and thus altering the fate of the adult-born stem cell lineage. In our model, NSCs accumulate under deprived conditions resulting in increased neurogenic potential when more favorable conditions return. Such cellular plasticity would provide additional computational units, potentially needed when enriched environments tax hippocampal function.

Experimental Procedures

Generation of nestin-CreER^{T2}/R26R-YFP mice

The CreERT2 sequence was removed from pCreERT2 (AA2) (Feil et al., 1997) a generous gift from P. Chambon) by EcoRI and inserted into the XhoI of pNerv-SXN (Josephson et al., 1998) a generous gift from R. Josephson). Orientation of the gene was confirmed by

sequencing. Nestin-CreERT2 transgenic mice were created by pronuclear injection of a SalI digest of pNerv-SXN-CreERT2 into fertilized embryos. Nestin-CreERT2 animals were bred with R26R enhanced yellow fluorescent protein (EYFP) reporter mice (Srinivas et al., 2001). All genotypes were confirmed by PCR.

Adminstration of Tamoxifen (TMX) and Bromodeoxyuridine (BrdU)

Animals aged 8–12 weeks were administered 5mg of tamoxifen (Sigma, St. Louis, MO) suspended in 100μL 1:1 honey:water mixture by gavage once a day for 4–5 days; or twice, 12h apart (experiments 1F–K, 2, 3F, S2A, S3). Animals were administered TMX in their home cages and then placed in their experimental environments. X-irradiated animals were administered TMX while undergoing enrichment. Animals were administered BrdU (150mg/kg IP) once with the first TMX administration (1F–K), twice with the final 2 TMX administrations (S3), and on four consecutive days (S6A,B).

Animal Housing

Standard-housed animals were kept in standard laboratory cages, 4–5 animals per cage, and sacrificed 24h (n=3), 48h (n=5), 5 days (n=3), 2 weeks (n=2), 1 month (n=3, 4), 3 months (n=3), 6 months (n=3), or 12 months (n=6) after the first day of TMX. EEE conditions have been previously described (Meshi et al., 2006), however animals were housed 6 to an enriched cage. EEE animals were sacrificed 1 (n=3) or 3 (n=3) months after TMX. Socially isolated animals were individually housed and sacrificed 1 (n=4) or 3 (n=4) months after TMX. Animals in all housing conditions were provided with food and water *ad libitum*. All animal experiments were performed in accordance with the *Guide for the Care and Use of Laboratory Animals* and approved by the Columbia University and New York State Psychiatric Institute Animal Care and Use Committee.

X-irradiation

Mice were anesthetized with 120mg/kg ketamine plus 8mg/kg xylazine (Phoenix Pharmaceuticals, St. Joseph, MO) diluted in sterile saline. Animals were placed in a stereotaxic frame with the top of the head resting 30cm below the X-ray source. A lead shield protected the body of the animals. Animals (n=5) were exposed to cranial irradiation using a Siemens Stabilopan X-ray system operated at 300 kVp and 20mA. X-rays were delivered one time for 5.5 mins, resulting in a dose of approximately 10 Gy. Dosimetry for this system has been reported elsewhere (Santarelli et al., 2003). Sham irradiated controls (n=2) received anesthesia only.

Sample Preparation

Animals were anesthetized as above and transcardially perfused with 4% paraformaldehyde (PFA). Brains were postfixed in 4% PFA overnight, cryoprotected in 30% sucrose, cryosectioned at 40μm, and stored in PBS with 0.02% sodium azide.

Immunohistochemistry

Free floating sections were washed in PBS, blocked and permeablized in 10% normal donkey serum and 0.5% triton X-100, and incubated overnight at 4°C in primary antibodies (except BLBP - 36h, and Nestin - 7d) in blocking solution.. For Nestin and BrdU, sections were mounted onto slides and antigen retrieval was performed. The following antibodies were used: Rabbit anti-BLBP (1:1000, gift from Dr. Nathaniel Heintz); Rat anti-BrdU (1:100, Serotec, Martinsried, Germany); Mouse anti-Calbindin (1:5000, Swant, Bellinzona, Switzerland); Rabbit anti-Cleaved Caspase-3 (1:500, Cell Signaling Technology, Beverly, MA); Goat anti-Doublecortin (1:500, Santa Cruz Biotechnology, Santa Cruz, CA); Rabbit anti-GFAP (1:1000, DAKO, Carpinteria, CA); Chicken anti-GFP (1:500, AbCam,

Cambridge, MA); Rabbit anti-GFP (1:1000, Molecular Probes, Eugene, OR); Goat anti-MCM2 (1:100, Santa Cruz Biotechnology, Santa Cruz, CA); Mouse anti-NeuN (1:1000, Chemicon, Temulca, CA); Rabbit anti-S100β (1:5000, Swant, Bellinzona, Switzerland); Rat anti-Nestin (1:50, BD Pharmingen, San Diego, CA); and Rabbit anti-Tbr2 (1:1000, AbCam, Cambridge, MA). All fluorescent secondary antibodies were obtained from Jackson ImmunoResearch (West Grove, PA) and diluted 1:400 in PBS except Goat anti-Rabbit Alexa 405 (1:200, Molecular Probes, Eugene, OR). Some sections were counterstained with Hoechst 33342 (1:10,000, Molecular Probes, Eugene, OR). For quadruple labeling, sequential secondary incubation was used to avoid cross-reactivity between Goat anti-Rabbit Alexa 405 with Goat anti-Doublecortin. The Cleaved Caspase-3 antibody was visualized using ABC and a DAB kits (Vector Laboratories, Burlingame, CA). Fluorescent confocal micrographs were captured with an Olympus IX81 confocal microscope equipped with a 405 laser and the aid of Olympus Fluoview 1000v1.5 software. Representative images were edited using Adobe Photoshop.

Identification of EYFP$^+$ neural stem cells

Three sections throughout the rostro-caudal extent of the dentate gyrus (anterior, middle, and posterior) were analyzed. EYFP$^+$GFAP$^+$ cells with radial astrocyte morphology were identified from 40X confocal micrographs under 150% digital zoom and assessed for co-expression of Nestin, MCM2, BLBP, or S100β. Over 360 EYFP$^+$GFAP$^+$ cells with radial morphology were quantified for expression of BLBP and S100β. For S100β cell counts in figures 2R and S9B, the Swant antibody was used. Fluorescent micrograph of S100β$^+$ cells in figure 2K,L was done with the Sigma antibody.

Unbiased stereology and lineage fate mapping

The total number of EYFP$^+$ cells were assessed in the dentate gyrus using the optical fractionator technique. Cells in every 6th atlas-matched, coronal section throughout the entire rostro-caudal axis of the hippocampus were counted unilaterally using a Zeiss Axioplan 2 microscope, MicroBrightField CX 900 digital camera, Ludl Electronic Products MAC 5000 motorized stage, and Stereoinvestigator version 7.2 software (MBF Bioscience, Willston, CT). Briefly, the dentate gyrus was outlined along the inner edge of the subgranular zone and 30μm from the outer edge of the granule cell layer in Hoechst-stained sections under 20X magnification. Since neurogenesis is most robust in the internal part of the DG, this approach was used to increase the homogeneity of target distribution and thus minimize ascertainment bias. An 80μm grid was projected over each section and EYFP$^+$ cell bodies were counted at 63X power in a sampling volume of 40μm × 40μm × 30μm for isolated and group housed animals, and 20μm × 20μm × 30μm for enriched animals. Cells lying within the top 10% of each section were excluded. This approach resulted in counting 150–400 cells in each brain yielding an average coefficient of error (Gundersen) of 0.062. Ratios of cells co-labeling with EYFP and NeuN, GFAP, or DCX were counted from confocal images of quadruple labeled sections. Three sections throughout the rostro-caudal extent of the dentate gyrus (anterior, middle, and posterior) were captured using a 40X objective. All EYFP$^+$ cells in 2 regions from the upper and 2 from the lower blade of the dentate gyrus from each section were assessed for co-expression of other markers in Fluoview software under 150% digital zoom. The absolute number of cells within each population was calculated by multiplying the population ratio by the absolute number of EYFP$^+$ cells as determined by stereology. The EYFP$^+$ NSC-derived lineage was estimated to contribute approximately 50% of all DCX$^+$ neurons born after TMX administration by dividing the number of EYFP$^+$DCX$^+$ cells by the total number of DCX$^+$ cells from the same sections. This ratio was similar across the 1-, 3-, and 6-months time points.

Statistical analyses

Statistical analyses were performed using ANOVA or two-tailed t-tests (paired and unpaired). One-tailed t-tests were used to compare the effects of environmental manipulations since the direction of change was expected. Linear fit was calculated for regression analysis. Animals from the 1, 3, and 6-month time points were pooled for regression analyses. All analyses were carried out using SPSS software (Chicago, IL; version 16.0). Statistical significance was defined as $p < 0.05$. Data are reported as mean ± SEM.

Supplementary Material

Refer to Web version on PubMed Central for supplementary material.

Acknowledgments

The authors thank Matheus Araujo for technical assistance, Eric Kandel and Harshad Vishwasrao for sharing confocal resources, Richard Josephson for providing the pNerv-SXN construct, Linda Byrd for assistance with mice, and Frank Gonzalez. We are grateful to Chris Henderson, Fiona Doetsch, Ben Samuels, and Jesse Richardson-Jones for helpful discussions and critical reading of the manuscript. This work was supported by NIH K08MH079088, BRAINS R01MH0911844, and NARSAD Young Investigator Awards (AD); NIH R01MH068542 and NYSTEM (RH); NCI CCR Intramural Research Program (SK), P50 MH66171 (Molecular and Cellular Core) and the NYSTEM institutional development award; AP was supported by NIH T32HD055165.

References

Abusaad I, MacKay D, Zhao J, Stanford P, Collier DA, Everall IP. Stereological estimation of the total number of neurons in the murine hippocampus using the optical disector. J Comp Neurol. 1999; 408:560–566. [PubMed: 10340505]

Ahn S, Joyner AL. In vivo analysis of quiescent adult neural stem cells responding to Sonic hedgehog. Nature. 2005; 437:894–897. [PubMed: 16208373]

Airan RD, Meltzer LA, Roy M, Gong Y, Chen H, Deisseroth K. High-speed imaging reveals neurophysiological links to behavior in an animal model of depression. Science. 2007; 317:819–823. [PubMed: 17615305]

Anthony TE, Klein C, Fishell G, Heintz N. Radial glia serve as neuronal progenitors in all regions of the central nervous system. Neuron. 2004; 41:881–890. [PubMed: 15046721]

Breunig JJ, Arellano JI, Macklis JD, Rakic P. Everything that glitters isn't gold: a critical review of postnatal neural precursor analyses. Cell Stem Cell. 2007; 1:612–627. [PubMed: 18371403]

Carlen M, Cassidy RM, Brismar H, Smith GA, Enquist LW, Frisen J. Functional integration of adult-born neurons. Curr Biol. 2002; 12:606–608. [PubMed: 11937032]

Clayton E, Doupe DP, Klein AM, Winton DJ, Simons BD, Jones PH. A single type of progenitor cell maintains normal epidermis. Nature. 2007; 446:185–189. [PubMed: 17330052]

Clelland CD, Choi M, Romberg C, Clemenson GD Jr, Fragniere A, Tyers P, Jessberger S, Saksida LM, Barker RA, Gage FH, et al. A functional role for adult hippocampal neurogenesis in spatial pattern separation. Science. 2009; 325:210–213. [PubMed: 19590004]

Dayer AG, Ford AA, Cleaver KM, Yassaee M, Cameron HA. Short-term and long-term survival of new neurons in the rat dentate gyrus. J Comp Neurol. 2003; 460:563–572. [PubMed: 12717714]

Deisseroth K, Singla S, Toda H, Monje M, Palmer TD, Malenka RC. Excitation-neurogenesis coupling in adult neural stem/progenitor cells. Neuron. 2004; 42:535–552. [PubMed: 15157417]

Doetsch F. The glial identity of neural stem cells. Nat Neurosci. 2003; 6:1127–1134. [PubMed: 14583753]

Doetsch F, Hen R. Young and excitable: the function of new neurons in the adult mammalian brain. Curr Opin Neurobiol. 2005; 15:121–128. [PubMed: 15721754]

Dranovsky A, Hen R. Hippocampal neurogenesis: regulation by stress and antidepressants. Biol Psychiatry. 2006; 59:1136–1143. [PubMed: 16797263]

Drapeau E, Abrous ND. Stem cell review series: role of neurogenesis in age-related memory disorders. Aging Cell. 2008; 7:569–589. [PubMed: 18221417]

Encinas JM, Michurina TV, Peunova N, Park JH, Tordo J, Peterson DA, Fishell G, Koulakov A, Enikolopov G. Division-coupled astrocytic differentiation and age-related depletion of neural stem cells in the adult hippocampus. Cell Stem Cell. 2011; 8:566–579. [PubMed: 21549330]

Encinas JM, Vaahtokari A, Enikolopov G. Fluoxetine targets early progenitor cells in the adult brain. Proc Natl Acad Sci U S A. 2006; 103:8233–8238. [PubMed: 16702546]

Feil R, Wagner J, Metzger D, Chambon P. Regulation of Cre recombinase activity by mutated estrogen receptor ligand-binding domains. Biochem Biophys Res Commun. 1997; 237:752–757. [PubMed: 9299439]

Fuchs E. The tortoise and the hair: slow-cycling cells in the stem cell race. Cell. 2009; 137:811–819. [PubMed: 19490891]

Ghazizadeh S, Taichman LB. Multiple classes of stem cells in cutaneous epithelium: a lineage analysis of adult mouse skin. EMBO J. 2001; 20:1215–1222. [PubMed: 11250888]

Gould E, Cameron HA, Daniels DC, Woolley CS, McEwen BS. Adrenal hormones suppress cell division in the adult rat dentate gyrus. J Neurosci. 1992; 12:3642–3650. [PubMed: 1527603]

Hodge RD, Kowalczyk TD, Wolf SA, Encinas JM, Rippey C, Enikolopov G, Kempermann G, Hevner RF. Intermediate progenitors in adult hippocampal neurogenesis: Tbr2 expression and coordinate regulation of neuronal output. J Neurosci. 2008; 28:3707–3717. [PubMed: 18385329]

Ibi D, Takuma K, Koike H, Mizoguchi H, Tsuritani K, Kuwahara Y, Kamei H, Nagai T, Yoneda Y, Nabeshima T, et al. Social isolation rearing-induced impairment of the hippocampal neurogenesis is associated with deficits in spatial memory and emotion-related behaviors in juvenile mice. J Neurochem. 2008; 105:921–932. [PubMed: 18182044]

Imayoshi I, Sakamoto M, Ohtsuka T, Takao K, Miyakawa T, Yamaguchi M, Mori K, Ikeda T, Itohara S, Kageyama R. Roles of continuous neurogenesis in the structural and functional integrity of the adult forebrain. Nat Neurosci. 2008; 11:1153–1161. [PubMed: 18758458]

Jones PH, Simons BD, Watt FM. Sic transit gloria: farewell to the epidermal transit amplifying cell? Cell Stem Cell. 2007; 1:371–381. [PubMed: 18371376]

Josephson R, Muller T, Pickel J, Okabe S, Reynolds K, Turner PA, Zimmer A, McKay RD. POU transcription factors control expression of CNS stem cell-specific genes. Development. 1998; 125:3087–3100. [PubMed: 9671582]

Kempermann G, Chesler EJ, Lu L, Williams RW, Gage FH. Natural variation and genetic covariance in adult hippocampal neurogenesis. Proc Natl Acad Sci U S A. 2006; 103:780–785. [PubMed: 16407118]

Kempermann G, Gast D, Kronenberg G, Yamaguchi M, Gage FH. Early determination and long-term persistence of adult-generated new neurons in the hippocampus of mice. Development. 2003; 130:391–399. [PubMed: 12466205]

Kempermann G, Kuhn HG, Gage FH. Genetic influence on neurogenesis in the dentate gyrus of adult mice. Proc Natl Acad Sci U S A. 1997; 94:10409–10414. [PubMed: 9294224]

Kempermann G, Kuhn HG, Gage FH. Experience-induced neurogenesis in the senescent dentate gyrus. J Neurosci. 1998; 18:3206–3212. [PubMed: 9547229]

Kitamura T, Saitoh Y, Takashima N, Murayama A, Niibori Y, Ageta H, Sekiguchi M, Sugiyama H, Inokuchi K. Adult neurogenesis modulates the hippocampus-dependent period of associative fear memory. Cell. 2009; 139:814–827. [PubMed: 19914173]

Lagace DC, Whitman MC, Noonan MA, Ables JL, DeCarolis NA, Arguello AA, Donovan MH, Fischer SJ, Farnbauch LA, Beech RD, et al. Dynamic contribution of nestin-expressing stem cells to adult neurogenesis. J Neurosci. 2007; 27:12623–12629. [PubMed: 18003841]

Laplagne DA, Esposito MS, Piatti VC, Morgenstern NA, Zhao C, van Praag H, Gage FH, Schinder AF. Functional convergence of neurons generated in the developing and adult hippocampus. PLoS Biol. 2006; 4:e409. [PubMed: 17121455]

Leuner B, Gould E, Shors TJ. Is there a link between adult neurogenesis and learning? Hippocampus. 2006; 16:216–224. [PubMed: 16421862]

Li Y, Luikart BW, Birnbaum S, Chen J, Kwon CH, Kernie SG, Bassel-Duby R, Parada LF. TrkB regulates hippocampal neurogenesis and governs sensitivity to antidepressive treatment. Neuron. 2008; 59:399–412. [PubMed: 18701066]

Lu L, Bao G, Chen H, Xia P, Fan X, Zhang J, Pei G, Ma L. Modification of hippocampal neurogenesis and neuroplasticity by social environments. Exp Neurol. 2003; 183:600–609. [PubMed: 14552901]

Lugert S, Basak O, Knuckles P, Haussler U, Fabel K, Gotz M, Haas CA, Kempermann G, Taylor V, Giachino C. Quiescent and active hippocampal neural stem cells with distinct morphologies respond selectively to physiological and pathological stimuli and aging. Cell Stem Cell. 2010; 6:445–456. [PubMed: 20452319]

Malatesta P, Hack MA, Hartfuss E, Kettenmann H, Klinkert W, Kirchhoff F, Gotz M. Neuronal or glial progeny: regional differences in radial glia fate. Neuron. 2003; 37:751–764. [PubMed: 12628166]

Malberg JE, Eisch AJ, Nestler EJ, Duman RS. Chronic antidepressant treatment increases neurogenesis in adult rat hippocampus. J Neurosci. 2000; 20:9104–9110. [PubMed: 11124987]

Mandyam CD, Harburg GC, Eisch AJ. Determination of key aspects of precursor cell proliferation, cell cycle length and kinetics in the adult mouse subgranular zone. Neuroscience. 2007; 146:108–122. [PubMed: 17307295]

Meshi D, Drew MR, Saxe M, Ansorge MS, David D, Santarelli L, Malapani C, Moore H, Hen R. Hippocampal neurogenesis is not required for behavioral effects of environmental enrichment. Nat Neurosci. 2006; 9:729–731. [PubMed: 16648847]

Ming GL, Song H. Adult neurogenesis in the mammalian central nervous system. Annu Rev Neurosci. 2005; 28:223–250. [PubMed: 16022595]

Monje ML, Mizumatsu S, Fike JR, Palmer TD. Irradiation induces neural precursor-cell dysfunction. Nat Med. 2002; 8:955–962. [PubMed: 12161748]

Morrison SJ, Spradling AC. Stem cells and niches: mechanisms that promote stem cell maintenance throughout life. Cell. 2008; 132:598–611. [PubMed: 18295578]

Nakagawa T, Nabeshima Y, Yoshida S. Functional identification of the actual and potential stem cell compartments in mouse spermatogenesis. Dev Cell. 2007; 12:195–206. [PubMed: 17276338]

Noctor SC, Martinez-Cerdeno V, Ivic L, Kriegstein AR. Cortical neurons arise in symmetric and asymmetric division zones and migrate through specific phases. Nat Neurosci. 2004; 7:136–144. [PubMed: 14703572]

Ramirez-Amaya V, Marrone DF, Gage FH, Worley PF, Barnes CA. Integration of new neurons into functional neural networks. J Neurosci. 2006; 26:12237–12241. [PubMed: 17122048]

Sahay A, Hen R. Adult hippocampal neurogenesis in depression. Nat Neurosci. 2007; 10:1110–1115. [PubMed: 17726477]

Sahay A, Scobie KN, Hill AS, O'Carroll CM, Kheirbek MA, Burghardt NS, Fenton AA, Dranovsky A, Hen R. Increasing adult hippocampal neurogenesis is sufficient to improve pattern separation. Nature. 2011

Santarelli L, Saxe M, Gross C, Surget A, Battaglia F, Dulawa S, Weisstaub N, Lee J, Duman R, Arancio O, et al. Requirement of hippocampal neurogenesis for the behavioral effects of antidepressants. Science. 2003; 301:805–809. [PubMed: 12907793]

Saxe MD, Battaglia F, Wang JW, Malleret G, David DJ, Monckton JE, Garcia AD, Sofroniew MV, Kandel ER, Santarelli L, et al. Ablation of hippocampal neurogenesis impairs contextual fear conditioning and synaptic plasticity in the dentate gyrus. Proc Natl Acad Sci U S A. 2006; 103:17501–17506. [PubMed: 17088541]

Seki T, Arai Y. Age-related production of new granule cells in the adult dentate gyrus. Neuroreport. 1995; 6:2479–2482. [PubMed: 8741746]

Seri B, Garcia-Verdugo JM, Collado-Morente L, McEwen BS, Alvarez-Buylla A. Cell types, lineage, and architecture of the germinal zone in the adult dentate gyrus. J Comp Neurol. 2004; 478:359–378. [PubMed: 15384070]

Srinivas S, Watanabe T, Lin CS, William CM, Tanabe Y, Jessell TM, Costantini F. Cre reporter strains produced by targeted insertion of EYFP and ECFP into the ROSA26 locus. BMC Dev Biol. 2001; 1:4. [PubMed: 11299042]

Stranahan AM, Khalil D, Gould E. Social isolation delays the positive effects of running on adult neurogenesis. Nat Neurosci. 2006; 9:526–533. [PubMed: 16531997]

Tashiro A, Makino H, Gage FH. Experience-specific functional modification of the dentate gyrus through adult neurogenesis: a critical period during an immature stage. J Neurosci. 2007; 27:3252–3259. [PubMed: 17376985]

Taupin P. BrdU immunohistochemistry for studying adult neurogenesis: paradigms, pitfalls, limitations, and validation. Brain Res Rev. 2007; 53:198–214. [PubMed: 17020783]

Toni N, Laplagne DA, Zhao C, Lombardi G, Ribak CE, Gage FH, Schinder AF. Neurons born in the adult dentate gyrus form functional synapses with target cells. Nat Neurosci. 2008; 11:901–907. [PubMed: 18622400]

Tozuka Y, Fukuda S, Namba T, Seki T, Hisatsune T. GABAergic excitation promotes neuronal differentiation in adult hippocampal progenitor cells. Neuron. 2005; 47:803–815. [PubMed: 16157276]

van Praag H, Kempermann G, Gage FH. Running increases cell proliferation and neurogenesis in the adult mouse dentate gyrus. Nat Neurosci. 1999; 2:266–270. [PubMed: 10195220]

van Praag H, Schinder AF, Christie BR, Toni N, Palmer TD, Gage FH. Functional neurogenesis in the adult hippocampus. Nature. 2002; 415:1030–1034. [PubMed: 11875571]

Wu CW, Chang YT, Yu L, Chen HI, Jen CJ, Wu SY, Lo CP, Kuo YM. Exercise enhances the proliferation of neural stem cells and neurite growth and survival of neuronal progenitor cells in dentate gyrus of middle-aged mice. J Appl Physiol. 2008; 105:1585–1594. [PubMed: 18801961]

Ying QL, Wray J, Nichols J, Batlle-Morera L, Doble B, Woodgett J, Cohen P, Smith A. The ground state of embryonic stem cell self-renewal. Nature. 2008; 453:519–523. [PubMed: 18497825]

Zhao C, Deng W, Gage FH. Mechanisms and functional implications of adult neurogenesis. Cell. 2008; 132:645–660. [PubMed: 18295581]

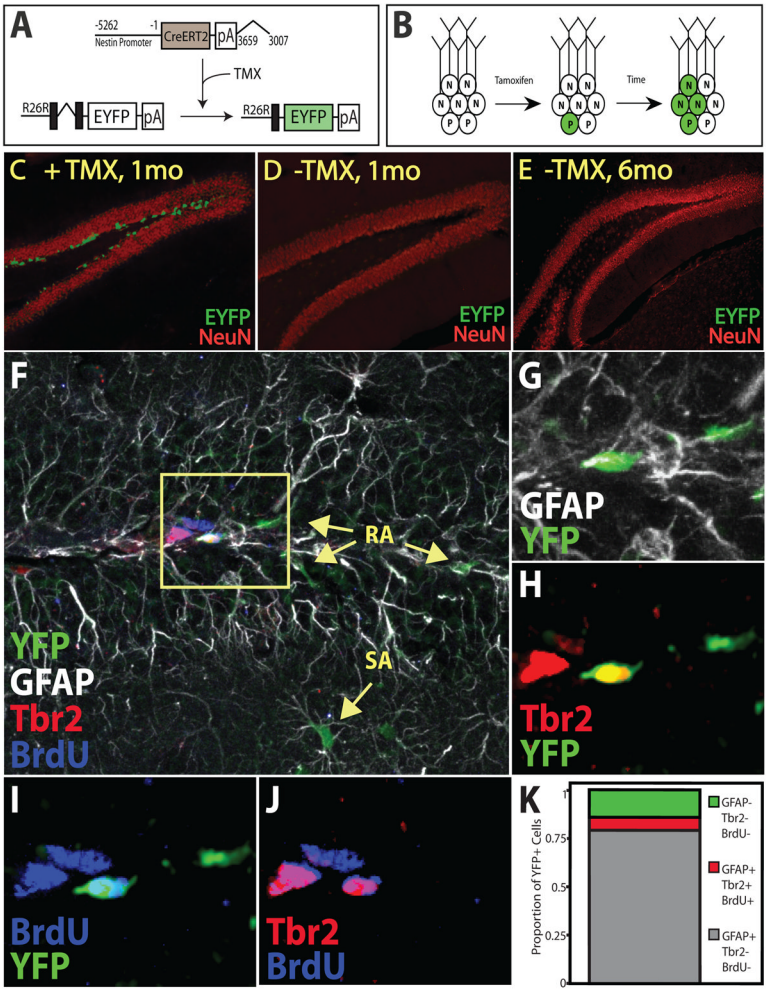

Figure 1. Inducible restriction of EYFP to Nestin-expressing neural stem cells (NSCs)

(**A**) Administration of tamoxifen (TMX) to NestinCreERT2/Rosa26-Stop-EYFP animals results in nuclear translocation of CreERT2 in Nestin-expressing cells, excision of the stop cassette, and constitutive expression of EYFP (green). (**B**) TMX administration results in constitutive EYFP expression by increasing numbers of NSCs, intermediate progenitors (P), and neurons (N) over time. (**C–E**) EYFP expression in bi-transgenic animals 1 month after TMX-mediated recombination (**C**), or 1 (**D**) and 6 (**E**) months after vehicle treatment. **(F–G)** Confocal micrographs of brains from NestinCreERT2/Rosa26-Stop-EYFP animals 48 hours after administration of tamoxifen and BrdU quadruple labeled for YFP, GFAP, Tbr2, and BrdU. YFP^+ cells were in the SGZ and, the molecular layers and were largely $GFAP^+$ radial (RA) or stellate (SA) cells **(F). (G)** Magnified inset and **(K)** quantification depict that most YFP^+ cells were $GFAP^+Tbr2^-BrdU^-$. All of the few identified YFP^+TBr2^+ cells were simultaneously $GFAP^+$ and $BrdU^+$ **(G–K)** indicating that Tbr2 expression is not limited to progenitors but initiates in NSCs at the time of division and that recombination occurs in $GFAP^+$ NSCs, but not $Tbr2^+$ progenitors. Many of the $Tbr2^+$ and few of the $GFAP^+$ cells were $BrdU^+$ **(J)** indicating that progenitors divide more frequently than NSCs or astrocytes.

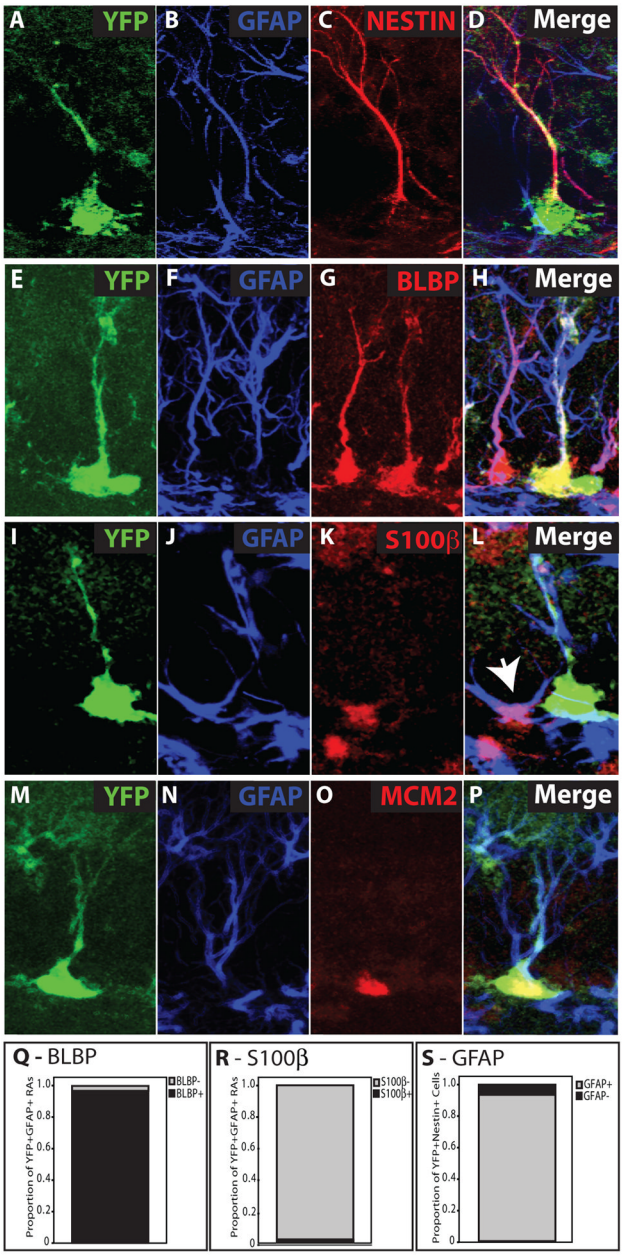

Figure 2. Identification of EYFP$^+$ Neural Stem Cells

Confocal micrographs depict EYFP$^+$ cells with radial **(A, E, I, M)** morphology. These EYFP$^+$ radial cells also express GFAP **(B,F,J,N)** in the radial process **(D, H, L, P)**. Nestin$^+$EYFP$^+$ cells are almost all GFAP$^+$ and exhibit radial morphology 6 days after TMX **(A–D, S)**. EYFP$^+$GFAP$^+$ radial cells co-label with the stem cell marker BLBP **(G, H)**, but not with the non-stem astrocyte marker S100β **(K, L)**. Non-radial, stellate cells co-label with S100β and GFAP (**L**, white arrow). EYFP$^-$GFAP$^+$BLBP$^+$ radial cells and EYFP$^-$GFAP$^+$S100β$^+$ stellate cells are readily detected **(H, L)**. However, nearly all EYFP$^+$GFAP$^+$ radial cells also express BLBP **(Q)**, while almost none express S100β **(R)**. Some EYFP$^+$GFAP$^+$ radial cells co-label with the cell division marker MCM2 **(O, P)**

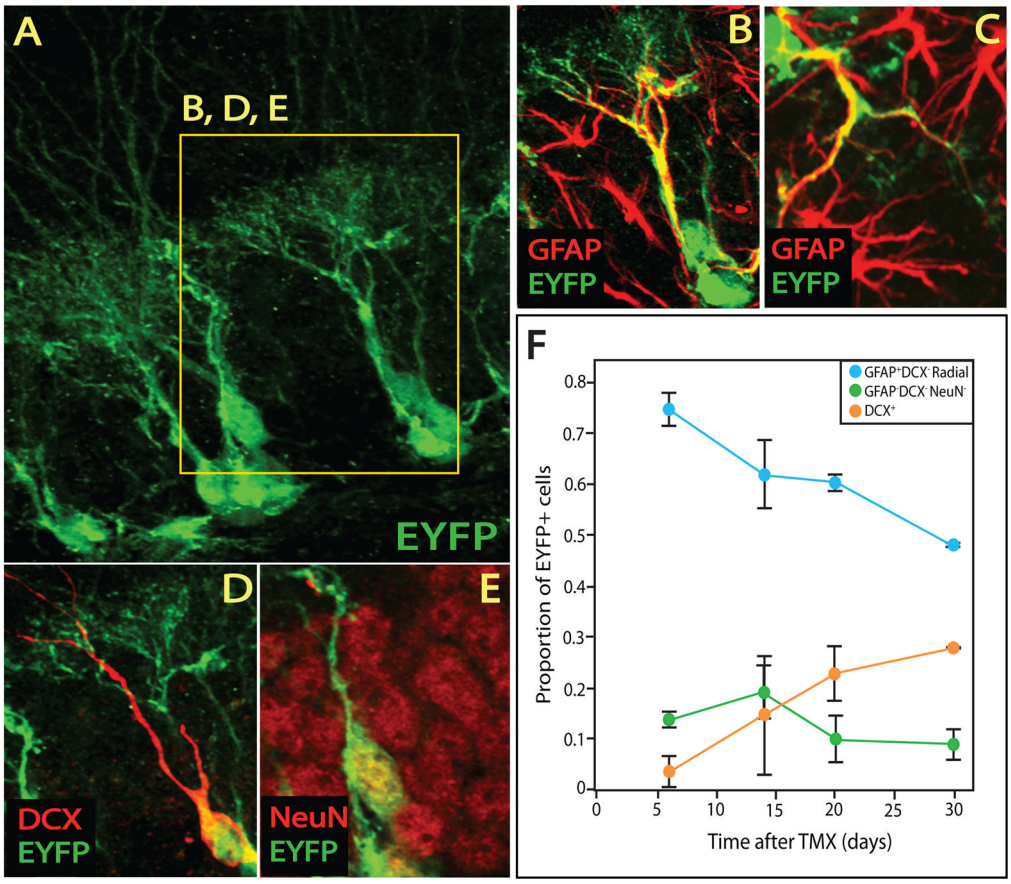

Figure 3. Defining the cellular components of the EYFP$^+$ neural stem cell lineage

(**A–E**) Confocal micrographs reveal that EYFP$^+$ cells (**A**) also express GFAP (**B,C**), DCX (**D**), and NeuN (**E**). EYFP$^+$GFAP$^+$ cells display morphology typical of either NSCs (**B**) or stellate astrocytes (**C**). DCX$^+$ immature neurons (**D**) and NeuN$^+$DCX$^-$ mature neurons (**D**,**E**) are also present within the EYFP$^+$ lineage. (**F**) Fate mapping analysis of EYFP$^+$ cells following a brief TMX administration protocol reveals that GFAP$^+$DCX$^-$NeuN$^-$ NSCs are the predominant cell type present 5 days after TMX and progressively decrease as GFAP$^-$DCX$^+$ cells appear over time. EYFP$^+$GFAP$^-$DCX$^-$NeuN$^-$ round cells are also present at all time points.

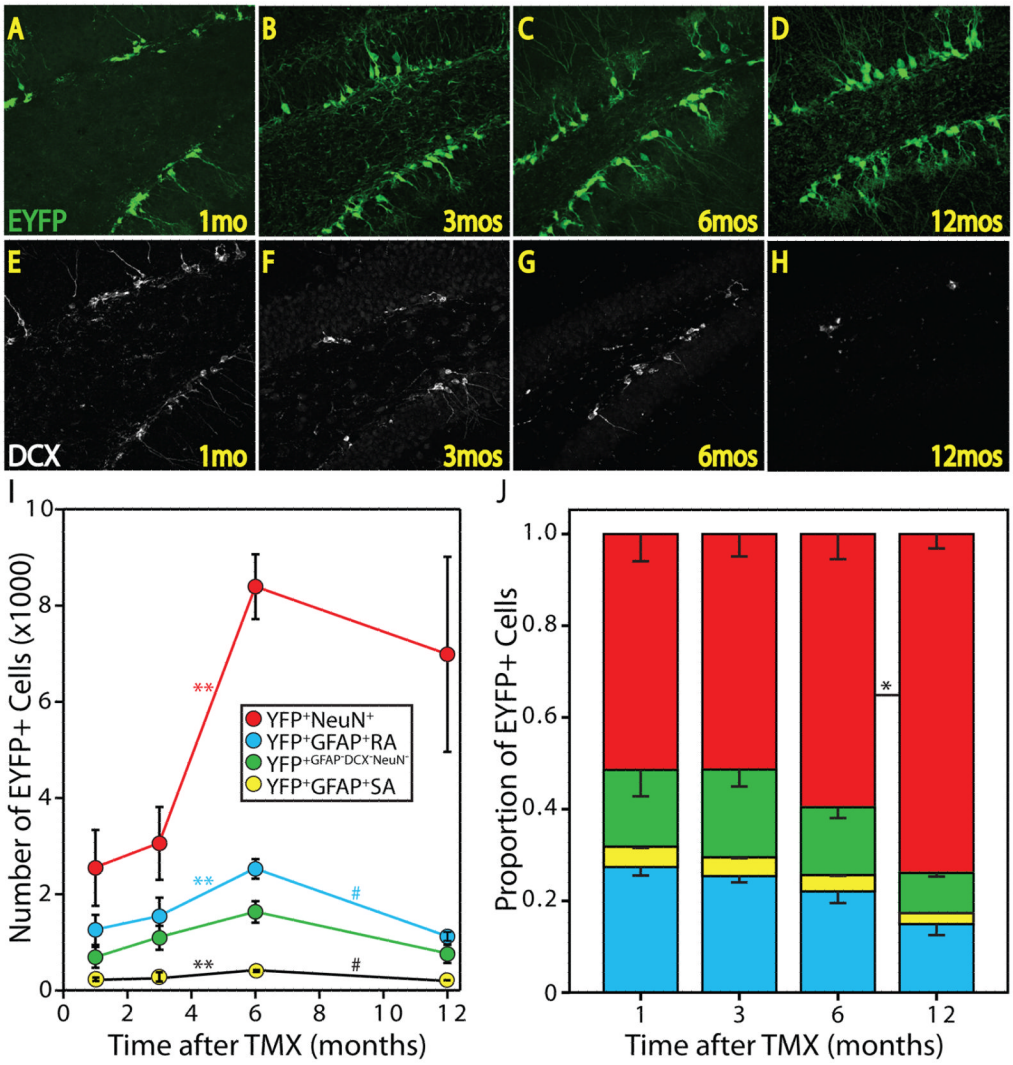

Figure 4. Lineage tracing and fate mapping of adult-born EYFP$^+$ cells

Confocal micrographs reveal EYFP$^+$ cells 1 (**A**), 3 (**B**), 6 (**C**), and 12 (**D**) months after TMX administration. DCX expression is highest 1 month after TMX (**E**), when the animals are youngest, and decreases between 1 (**E**) and 3 (**F**) months, and 6 (**G**) and 12 (**H**) months time points. Note the abundance of EYFP$^+$ cells 12 months after TMX (**D**) when few DCX$^+$ cells are present (**H**). (**I**) Stereological analysis and fate-mapping of the EYFP$^+$ lineage with reveal that NSCs, astrocytes, and neurons accumulate from 3 to 6 months after TMX administration. A decrease in NSCs and astrocytes occurs between 6 and 12 months and is accompanied by an increase in variance in neurons (**p<0.01, #p≤0.001). (**J**) The proportion of NSCs, astrocytes, neurons, intermediate progenitors and other cellular populations within the EYFP$^+$ lineage. Note that the ratio of each cell type is not different between time points until 12 months after TMX, when neurons represent a greater proportion of the lineage than at the 6-months time point (*p<0.05). 1 (n=4); 3 (n=3); 6 (n=3); 12 (n=6) months.

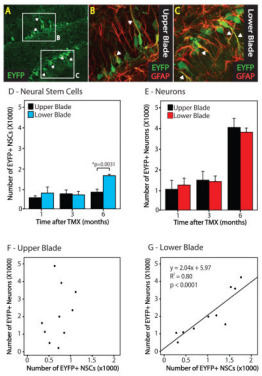

Figure 5. The NSC-neuron relationship differs between blades of the dentate gyrus

(**A**) A confocal micrograph depicts a similar number of EYFP$^+$ cells between upper and lower blades of the dentate 6 months after TMX. Higher magnification reveals more EYFP$^+$GFAP$^+$ radial NSCs present in the lower blade (**C**) compared to the upper blade (**B**). (**D**) Stereological analysis and fate mapping reveal that more EYFP$^+$ NSCs are present in the lower blade than the upper blade at 6 months following TMX. (**E**) No difference in the number of neurons is observed between blades. There is a linear relationship between NSCs and the number of neurons they produced in the lower (**G**, $p<0.0001$), but not the upper (**F**) blade of the dentate across all time points. 1(n=4); 3(n=3); 6(n=3) months.

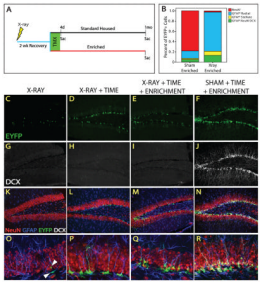

Figure 6. X-irradiation obliterates neurogenesis but not stem cell accumulation

(**A**) Animals were subjected to sham or X-irradiation, allowed 2 weeks recovery, exposed to standard or enriched (EEE) housing, and treated with TMX. Animals were sacrificed immediately after TMX (standard housed only) or after 1 month of standard housing or EEE. (**B**) The proportion of cellular populations within the $EYFP^+$ lineage in a representative sham and x-irradiated EEE animal. The majority of $EYFP^+$ cells are neurons in sham-, and NSCs in X-irradiated animals. Confocal micrographs reveal the lack of DCX after X- (**G–I**) but not sham irradiation (**J**), indicating that DCX is not expressed in the irradiated brain. (**C, K, O**) X-irradiation does not obliterate all $EYFP^+$ cells. (**O**) Surviving $EYFP^+$ cells are $GFAP^+$ and exhibit mainly NSC morphology. Some stellate $GFAP^+EYFP^+$ cells are also present. There are more $EYFP^+$ cells in X-irradiated animals 1 month after TMX (**D,L,P**) and most cells are $GFAP^+$ NSCs (**P**). The number of $EYFP^+$ cells is similar in EEE (**E, M**) and standard housed (**D, L**) X-irradiated animals. (**P, Q**) Radial processes are more tortuous in NSCs of EEE X-irradiated animals than EEE shams. Higher magnification reveals that most $EYFP^+$ cells are $GFAP^+$ and display radial morphology in X-irradiated (**O–Q**), but not sham (**R**) animals.

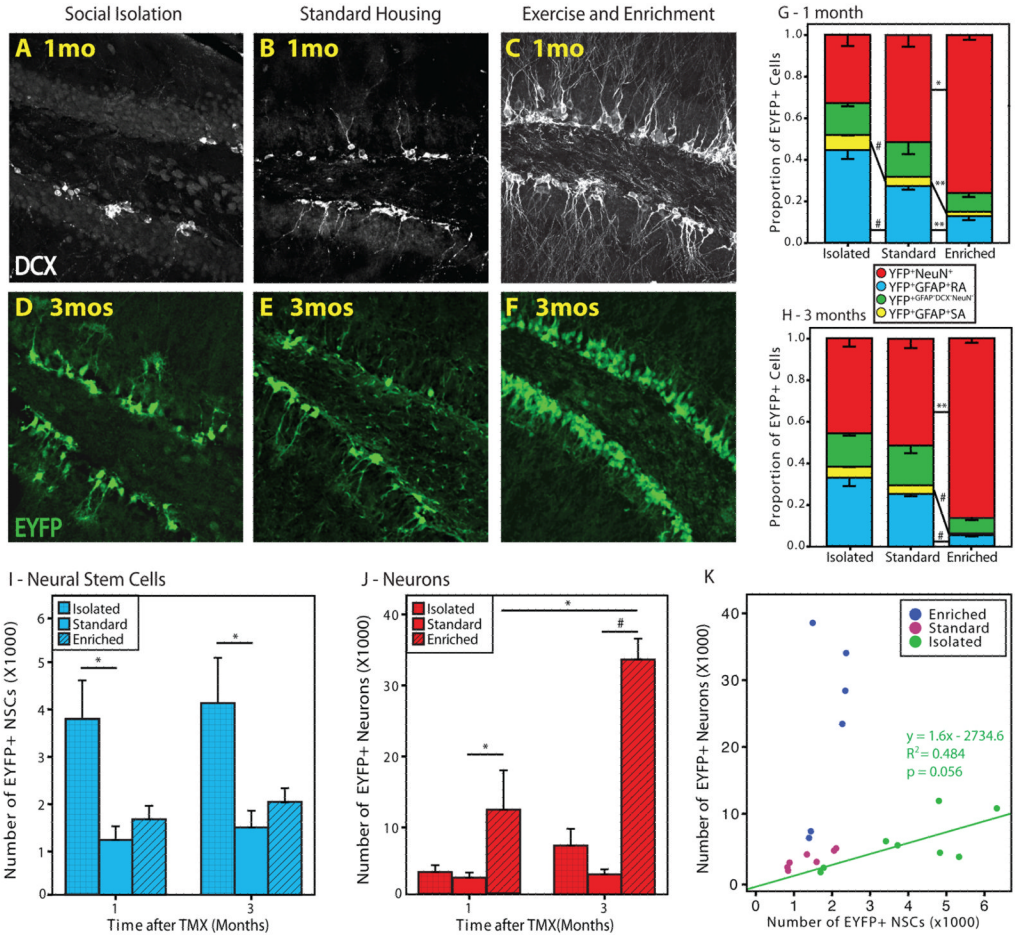

Figure 7. Social isolation and enrichment bi-directionally regulate fate of the NSC lineage

Confocal micrographs demonstrate a decrease in DCX^+ cells in isolated (**A**) and an increase in EEE (**C**) compared to standard-housed (**B**) animals. There are more $EYFP^+$ cells in isolated (**D**) and EEE (**F**) compared to standard housed (**E**) animals. (**G**) Exposure to 1 month of social isolation increases the proportion of $EYFP^+$ NSCs, while EEE increases the proportion of EYFP+ neurons compared to standard housed animals. (**H**) 3 months of EEE further increases the proportion of $EYFP^+$ neurons, but no change occurs in the proportion of $EYFP^+$ NSCs due to social isolation after 3 months (*$p<0.05$; **$p<0.01$; #$p<0.001$). (**I**) Stereology reveals more $EYFP^+$ NSCs in isolated compared to standard-housed animals. (**J**) $EYFP^+$ neurons increased following EEE, with over 30,000 counted after 3 months. (**K**) There is a linear relationship between NSCs and neurons in isolated, but not in standard housed or EEE animals. Relatively few NSCs give rise to many neurons in EEE animals. 1 month standard housed (n=4), isolated (n=4), EEE (n=3); 3 months standard housed (n=3), isolated (n=4), EEE (n=3).

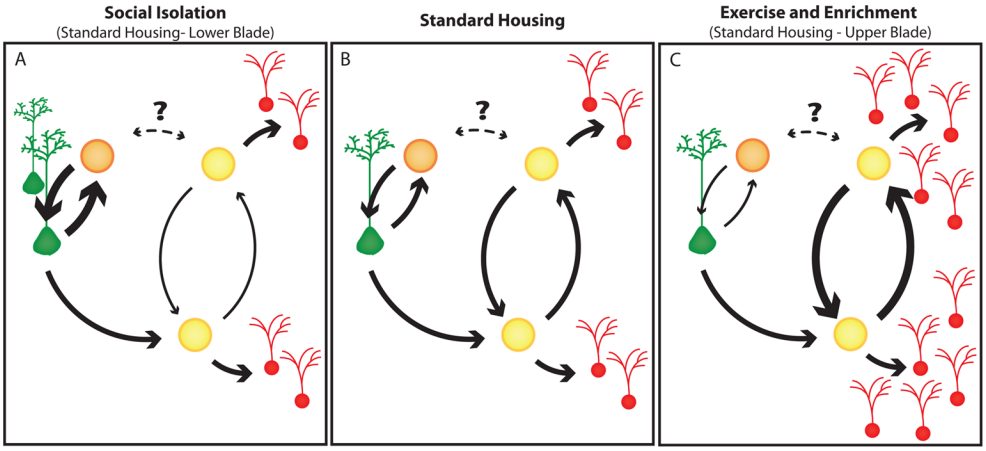

Figure 8. A model for homeostasis of adult hippocampal neurogenesis

(**B**) In standard housed animals, NSCs (green) divide to produce 2 IPs (yellow and orange). An IP can divide to produce either two IPs, an IP (yellow) and a neuron (red), or an IP (orange) and another NSC. It is unclear whether IPs are multipotent with regard to neurogenesis and NSC proliferation or if two distinct IP types are present (i.e. whether orange and yellow represent the same or distinct cells.) The later possibility would be more consistent with the notion of symmetrically dividing NSCs. (**A**) Social isolation decreases the likelihood that IPs will increase in number resulting in a linear relationship between NSCs and neurons. The IPs do not serve as a transit-amplifying cell in this case. Increased likelihood of NSC production in this case results in increased numbers of NSCs. A similar effect is observed in the lower blade of the dentate in standard-housed animals. (**C**) Enrichment promotes increase in the number of IPs, resulting in a variable relationship between NSCs and neurons characteristic of transit-amplifying IP cells. These cells eventually terminally differentiate with greater probability into neurons. A similar effect is observed in the upper blade of the dentate gyrus in standard housed animals. X-irradiation preferentially ablates rapidly proliferating IPs, but not less frequently dividing NSCs, and permanently disrupts only the neurogenic niche.